

EARTHQUAKE REPORT

24 MAY 2014 NORTHERN AEGEAN SEA

1. General Information

An earthquake with $M_I=6.5$ occurred in the Northern Aegean on 24 May 2014 12:25 local time (UTC +3) approximately 30 km north-west of Gökçeada (Imbros) Island resulting in strong ground motion in the region. The focal depth of the earthquake is 23 km and considered as shallow. The earthquake has been felt in Marmara and Aegean regions of Turkey, primarily in Çanakkale, Balıkesir, Edirne and Istanbul.

The magnitude of the earthquake has been calculated as $M_I=6.5$ based on the comparison of the recordings of the seismic stations operated by the National Earthquake Monitoring Center of KOERI and seismic stations operated by the Disaster and Emergency Management Presidency (DEMP) in consultation with DEMP.



Figure 1-1. Epicentral location of the Offshore Gökçeada (Imbros) – Northern Aegean Sea Earthquake ($M_I=6.5$)

This report has been prepared by KOERI with contributions from Mustafa Erdik, Ali Pinar, Sinan Akkar, Can Zülfiyar, Doğan Kalafat, Kivanç Kekovalı, Nurcan Meral Özel and Öcal Necmioğlu.

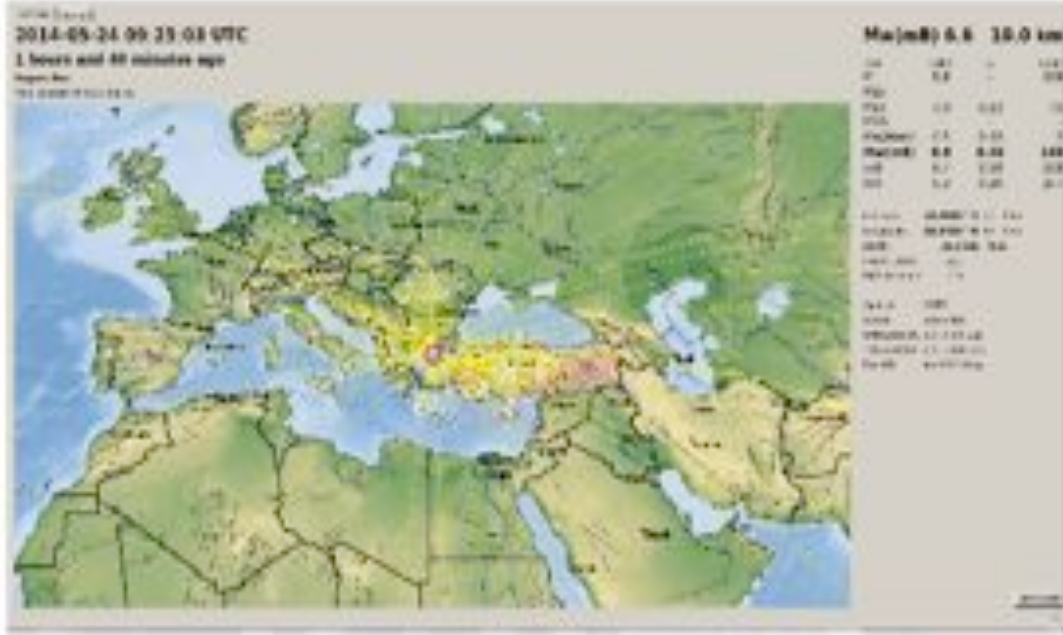


Figure 1-2. Automatic solution of the Offshore Gökçeada (Imbros) – Northern Aegean Sea Earthquake provided by SeisComp3

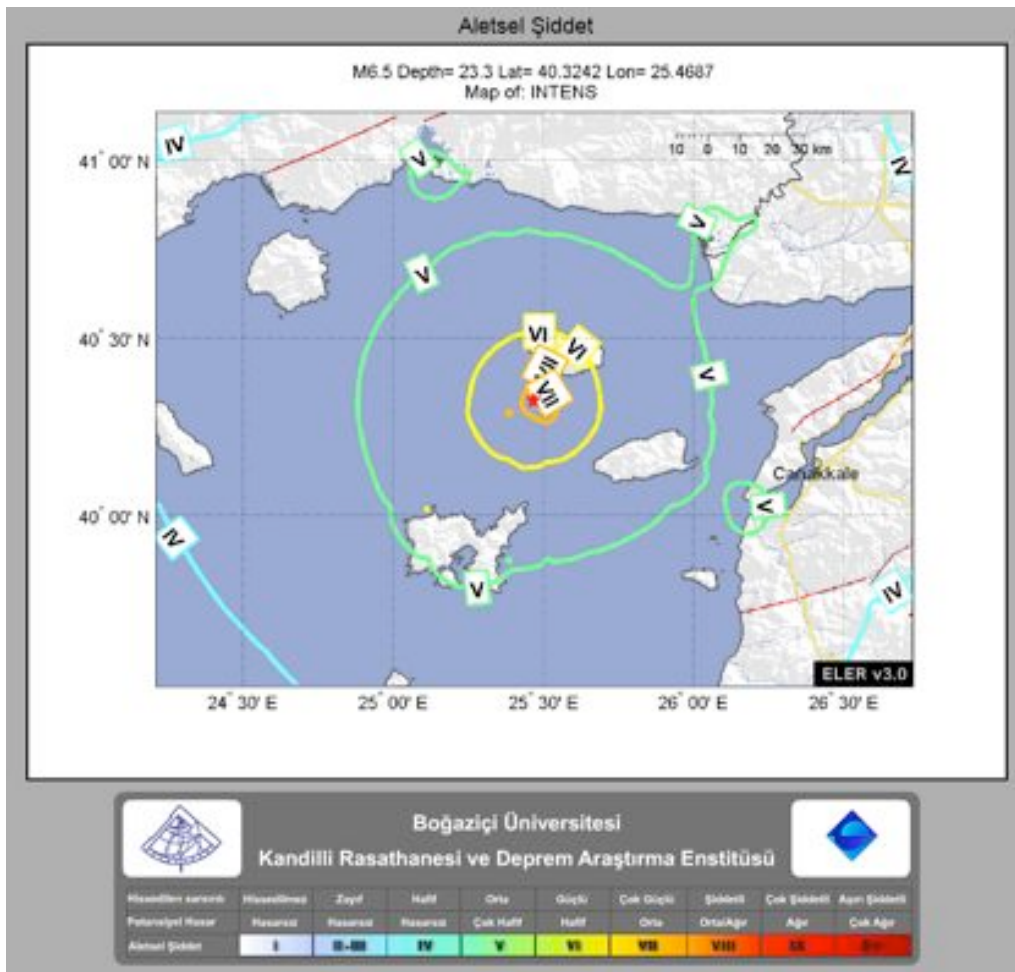


Figure 1-3. Intensity map automatically produced after the earthquake.

This report has been prepared by KOERI with contributions from Mustafa Erdik, Ali Pinar, Sinan Akkar, Can Zülfikar, Doğan Kalafat, Kivanç Kekovalı, Nurcan Meral Özel and Öcal Necmioğlu.

The epicentral intensity of the earthquake is VII, whereas the intensity at Çanakkale has been identified as V.

The region is the continuation of the North Anatolian Fault Zone (NAFZ) in tectonic terms and is within a tectonic regime that produces such medium-sized earthquakes.

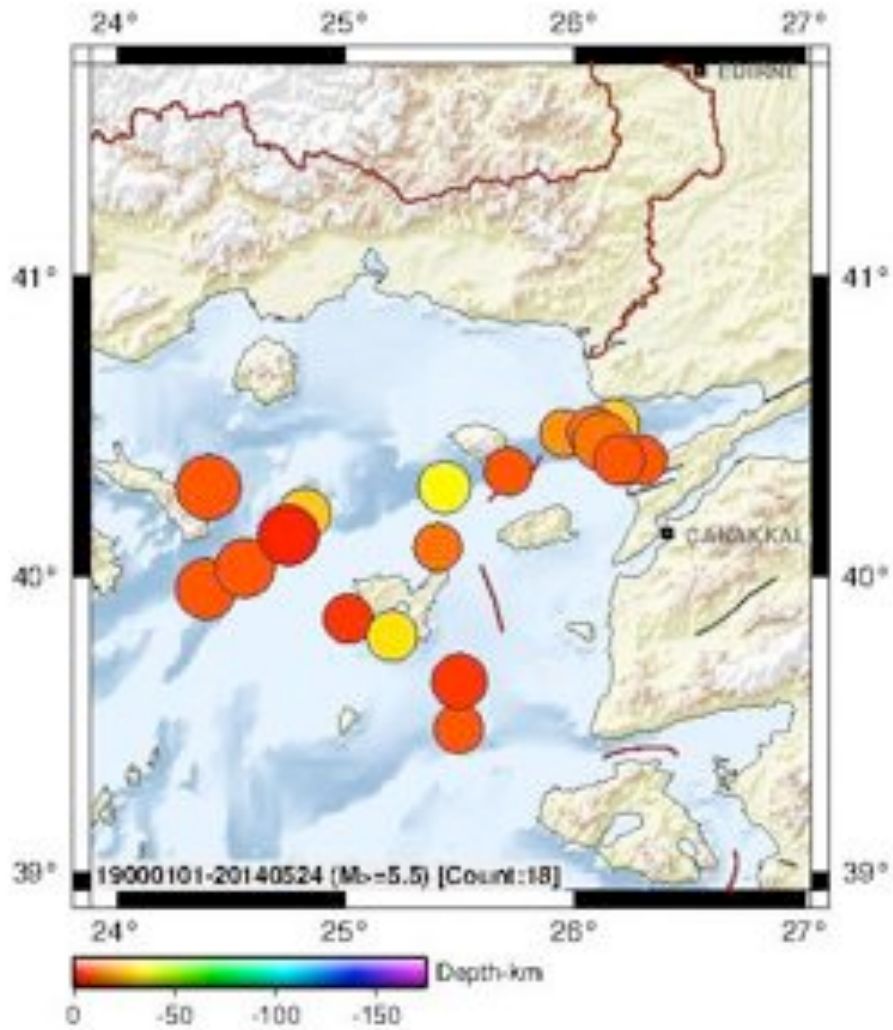


Figure 1-4. Location map of earthquakes since 1900 with instrumental magnitude of $M \geq 5.5$

In the near past, an earthquake of $M_I=6.2$ offshore Bozcaada (Tenedos) on 8 January 2013 and another one offshore Gökçeada (Imbros) with $M_I=5.3$ on 30 July 2013 occurred in the region.

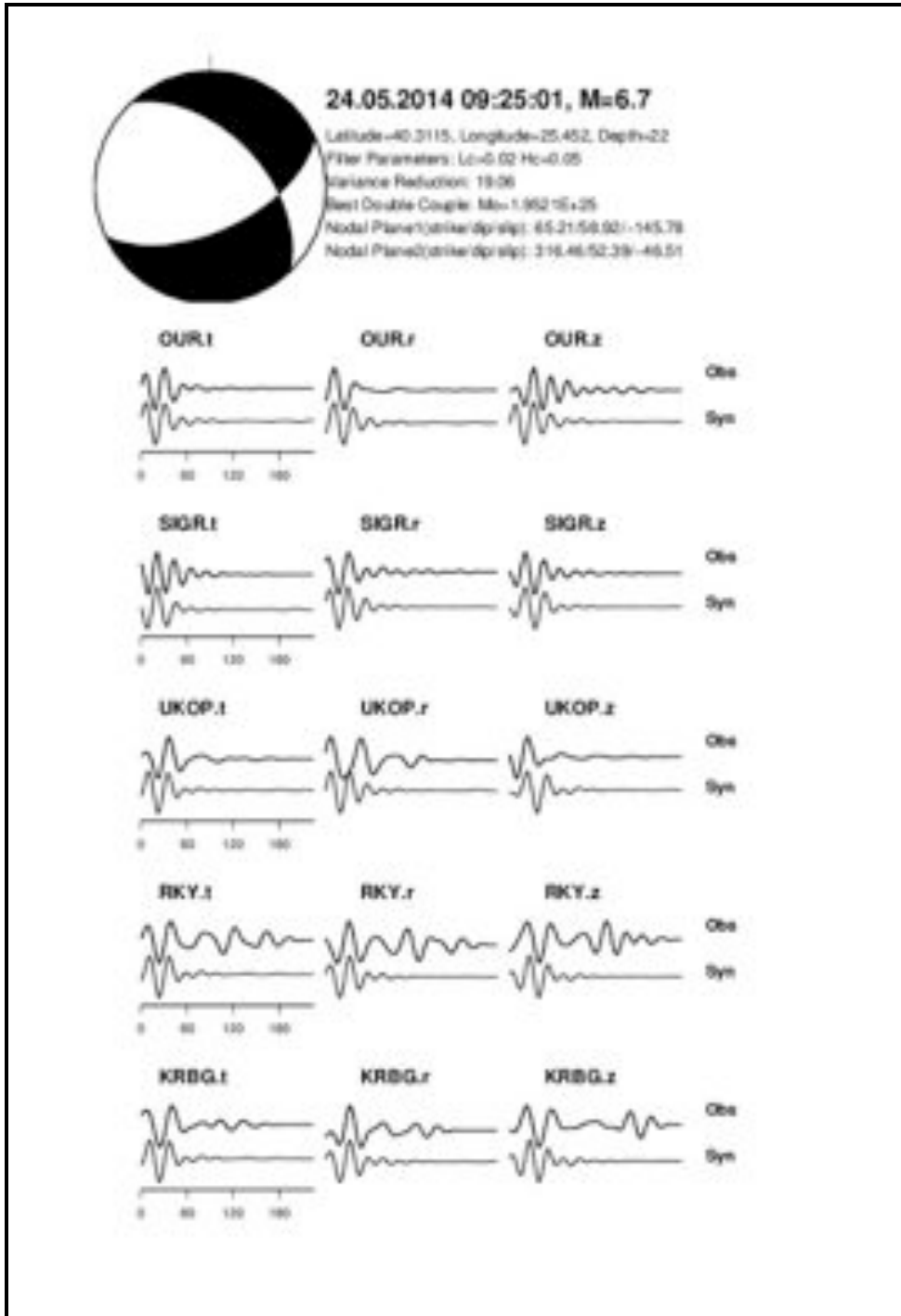


Figure 1-5. Focal mechanism solution of the 24 May 2014 Offshore Gökçeada (Imbros) – Northern Aegean Sea Earthquake (MI=6.5) obtained from MTI.

The earthquake occurred on a fault with a NE-SW strike, where the largest portion of the energy was released towards these directions. Hence, the earthquake was felt strongly in Çanakkale-Istanbul and their surroundings.

This report has been prepared by KOERI with contributions from Mustafa Erdik, Ali Pinar, Sinan Akkar, Can Zülfiyar, Doğan Kalafat, Kivanç Kekovalı, Nurcan Meral Özel and Öcal Necmioğlu.

2. Damage and Losses

On Saturday 24 May, a magnitude M6.5 earthquake struck in the Aegean Sea between the Greek islands of Samothraki and Lemnos, and close to the Turkish island of Gökçeada.

Strong ground shaking was widely felt across Turkey, Greece and Bulgaria including the major cities of Çanakkale, Thessaloniki, Edirne, Plovdiv, İzmir and İstanbul. However, with the exception of Çanakkale no damage has been reported in these cities. The maximum intensity of ground shaking felt on land was VI-VII on the EMS'98 scale. This level of shaking has the potential to cause light damage to buildings and moderate damage to vulnerable structures.

According to media reports, no major damage has been reported as a result of the earthquake, although hundreds of vulnerable buildings have sustained damage. Several hundred people in the region have been reported injured mostly the result of panic as people rushed out of buildings (Figure 2-1).

For more than half an hour following the earthquake, cellular phone service was unavailable in the Marmara region, due to extensive use immediately after the earthquake, according to a written statement from Information Technologies and Communications Authority (BTK) of Turkey. Turkish news media reports that the usage of messaging applications, such as the WhatsApp, increased dramatically while GSM service was out.

As reported by the Disaster and Emergency Management Presidency (AFAD), about 321 people were temporarily hospitalised, most with minor injuries. Most of the injuries were caused by people panicking during the earthquake and rushing out of their homes and even jumping from the balconies. AFAD reported that: in Çanakkale province the earthquake caused damage to about 300 buildings, about 50 of them located in the city of Çanakkale and 200 of them located in the island of Gökçeada (Figures 2-2, 2-3, 2-4 and 2-5). There were 8 school buildings with light damage. According to media reports, in the city center of Çanakkale three mosques received light damage mostly in the top of the minarets. Among those the Arslanca Mosque was closed to prayers, pending further assessment of damage (Figure 2-6). Furthermore, the earthquake caused cracking in the walls of Yenice state hospital in the province of Çanakkale. The patients were evacuated from the hospital, and a field hospital was constructed (Figure 2-7).

In the island of Lemnos, according to media reports, the earthquake caused the collapse of 11 uninhabited houses, two churches were damaged while there were minor damages in tens of houses and three schools. Significant damages have been recorded in the Myrina museum where dozens of exhibits fell on the floor. There was damage to the suspended ceiling of the Lemnos Airport (Figure 2-9).

Contents damage was widely reported with objects falling from shelves in the region, some as far as 250km away (Figure 2-10).

Turkish Compulsory Earthquake Insurance (TCIP-DASK) has a penetration of about 45% in the earthquake affected region, and about 500 claims are expected.

This report has been prepared by KOERI with contributions from Mustafa Erdik, Ali Pinar, Sinan Akkar, Can Zülfikar, Doğan Kalafat, Kivanç Kekovalı, Nurcan Meral Özel and Öcal Necmioğlu.



Figure 2-1. Residents of Edirne rushed to the street (After Cihan Haber Ajansı)



Figure 2-2. Damage at Gökçeada (After Doğan Haber Ajansı)



Figure 2-3. Damage to a Building at Gökçeada (After Haberciniz.biz)

This report has been prepared by KOERI with contributions from Mustafa Erdik, Ali Pınar, Sinan Akkar, Can Zülfikar, Doğan Kalafat, Kivanç Kekovalı, Nurcan Meral Özel and Öcal Necmioğlu.



Figure 2-4. Damage to a Building at Gökçeada (After Haberciniz.biz)



Figure 2-5. Damaged Building in a Çanakkale (After Cihan Haber Ajansı)



Figure 2-6. Minor Damage at Aslanca Mosque in Çanakkale (İhlas Haber Ajansı)

This report has been prepared by KOERI with contributions from Mustafa Erdik, Ali Pinar, Sinan Akkar, Can Zülfikar, Doğan Kalafat, Kivanç Kekovalı, Nurcan Meral Özel and Öcal Necmioğlu.



Figure 2-7. Lighty Damaged Hospital building and the field hospital installed



Figure 2-8. Damage to an old building in Lemnos Island (*After Protothema News*)



Figure 2-9. Suspended Ceiling Damage at Lemnos Airport (After Liz Fields (/contributor/liz-fields))



Figure 2-10. Damage to shelved items in a Market in Adapazarı (about 250km east of the epicenter) (After Cihan Haber Ajansı)

3. Earthquake Hazard and Loss Estimation

ELER (Earthquake Loss Estimation Routine) has been utilized for the Earthquake Hazard and Loss estimation studies. After the event the RT-ELER has automatically produced the intensity map of the event as shown in Figure 3-1 (www.kandilli.info). As it is shown from the Figure 3-1, the first intensity estimation of the event was VII in the epicentral region, VI in the nearby islands and V, IV on the Greek and Turkish coasts.



Figure 3-1. Near Real Time Intensity Map of the event by RT-ELER (www.kandilli.info).

The raw PGA values recorded at the accelerometric stations from Greek (ITSK) and Turkish (KOERI and AFAD) networks with their distances to the epicenter are given in Table-1, and their locations are shown in Figure 3-2.

Table 3-1. Accelerometer Stations Information in the region.

KOERI	ITSK	AFAD
-------	------	------

This report has been prepared by KOERI with contributions from Mustafa Erdik, Ali Pinar, Sinan Akkar, Can Zülfikar, Doğan Kalafat, Kivanç Kekovalı, Nurcan Meral Özel and Öcal Necmioğlu.

Station	Distance (km)	PGA(%g)	Station	Distance (km)	PGA(%g)	Station	Distance (km)	PGA(%g)
ENEZ	66.5	6.34	XAN2	100.6	1.19	2201	68.6	11.38
ERIK	98.2	6.57	THS1	81.6	8.69	1711	40.1	18.00
GELI	86.9	5.53	SPP1	82.6	4.45	1708	73.1	3.21
GADA	39.6	4.27	SGR1	121.2	1.07	1714	84.3	5.21
EZNO	91.1	2.44				1701	81.6	14.38
						1713	82.0	9.62



Figure 3-2. Location of Accelerometer Stations in the vicinity of the event with different networks.

The first PGA distribution estimation of the event has been achieved by RT-ELER without any station information as shown in Figure 3-3. Boore-Atkinson (2008) ground motion prediction equation has been used for this first estimation. The estimated PGA distribution has been bias-adjusted after the information from acceleration networks KOERI, ITSAK and AFAD were obtained. Figure 3-4, Figure 3-5 and Figure 3-6 show the bias adjusted PGA distribution with the information from KOERI, ITSAK and AFAD accelerometric networks.

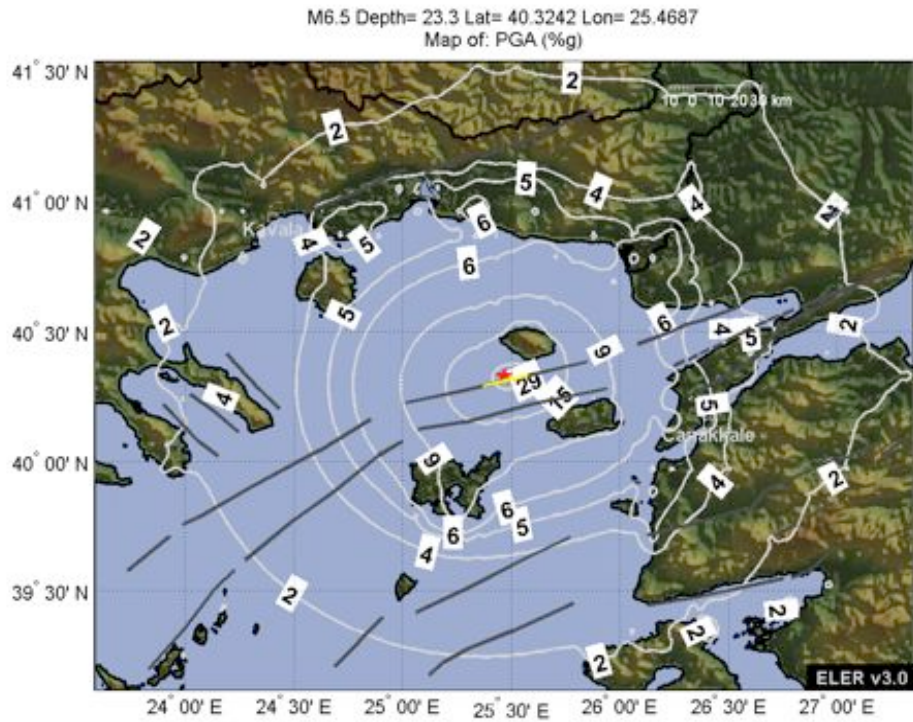


Figure 3-3. PGA distribution without station information.

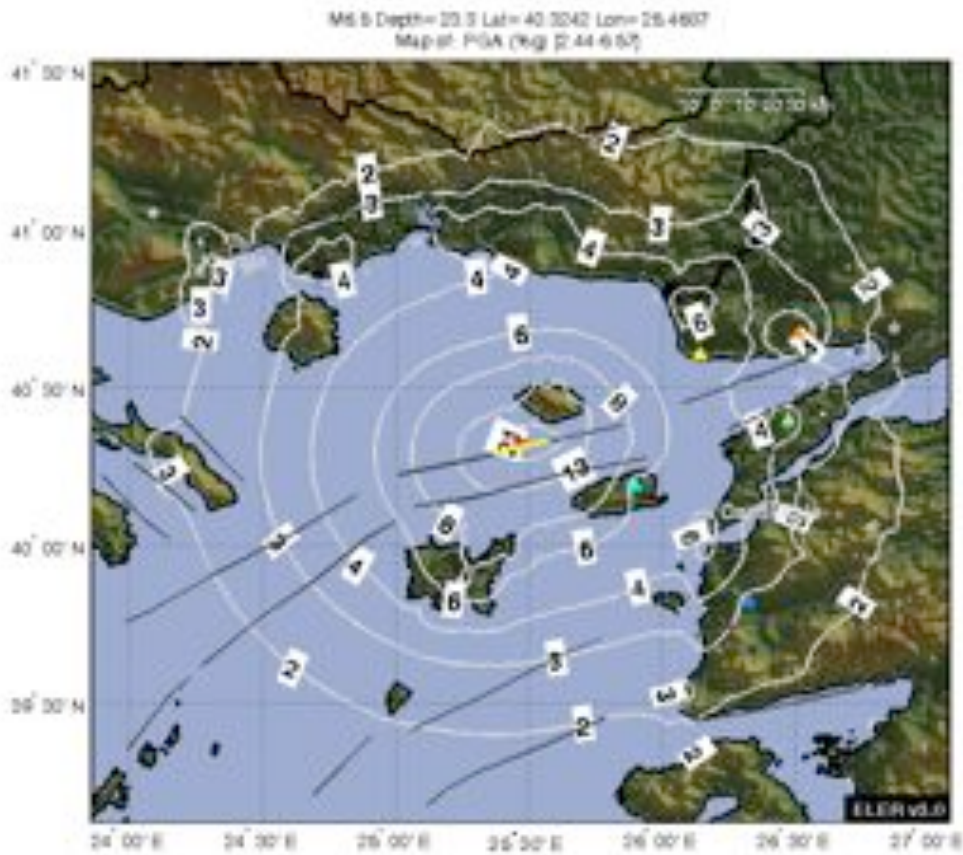


Figure 3-4. PGA distribution with information from KOERI network.

This report has been prepared by KOERI with contributions from Mustafa Erdik, Ali Pinar, Sinan Akkar, Can Zülfikar, Doğan Kalafat, Kivanç Kekovalı, Nurcan Meral Özel and Öcal Necmioğlu.

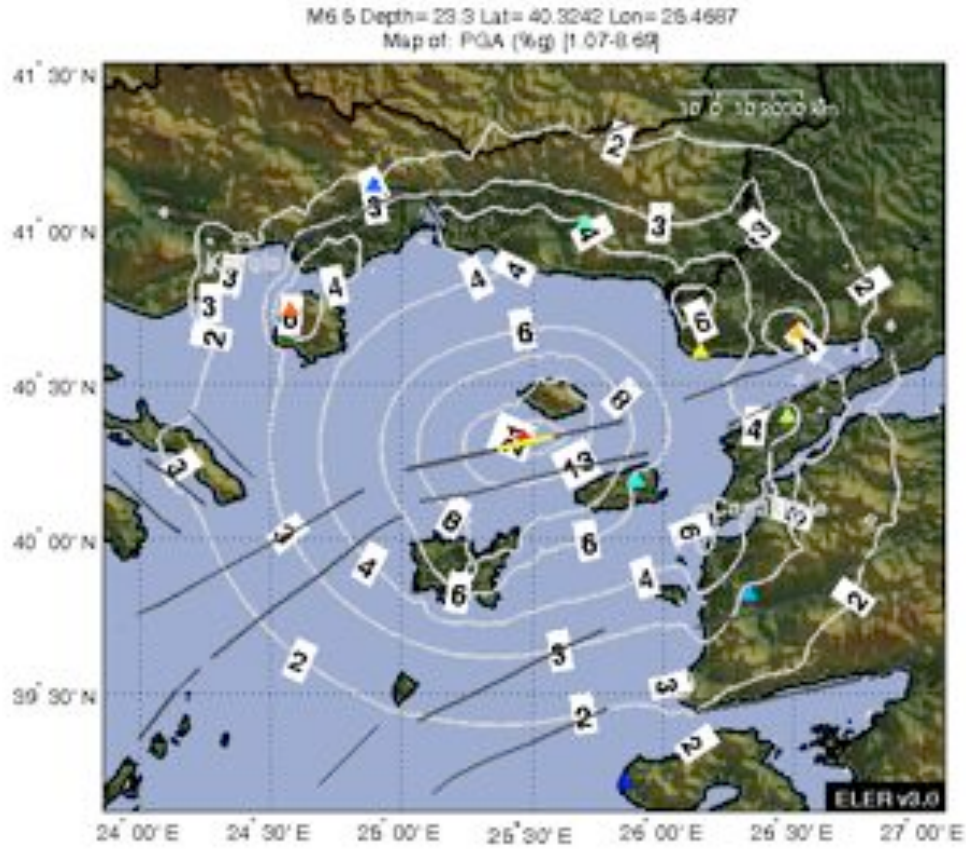


Figure 3-5. PGA distribution with information from ITSAK and KOERI networks.



Figure 3-6. PGA distribution with information from ITSAK, KOERI and AFAD networks.

This report has been prepared by KOERI with contributions from Mustafa Erdik, Ali Pinar, Sinan Akkar, Can Zulfikar, Doğan Kalafat, Kivanç Kekovalı, Nurcan Meral Özel and Öcal Necmioğlu.

Figure 3-7 and Figure 3-8 show the distribution of the Spectral Acceleration (Sa) at 0.2s and 1.0s periods.

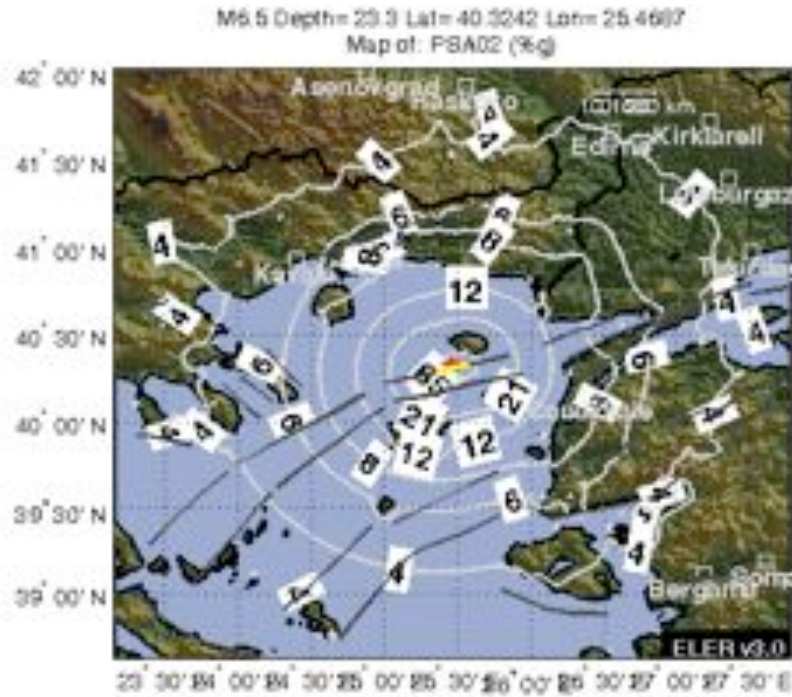


Figure 3-7. Sa at period 0.2s distribution in the epicentral region.

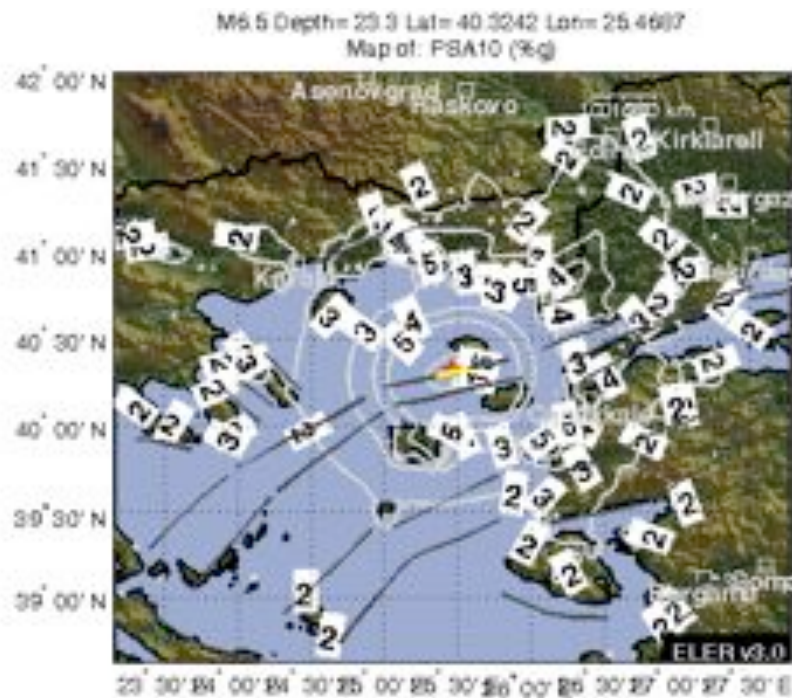


Figure 3-8. Sa at period 1.0s distribution in the epicentral region.

After the event, the building damage estimation analysis has been achieved by ELER for the epicentral region and Istanbul.

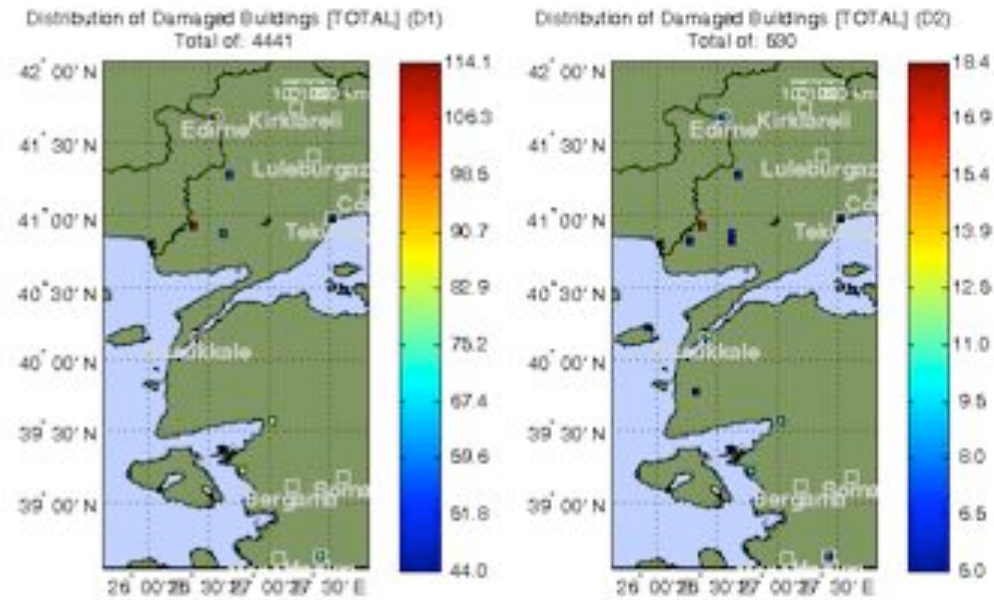


Figure 3-9. Number of Buildings with D1 (Slight Damage) and D2 (Moderate Damage) Levels on the left and right sides, respectively.

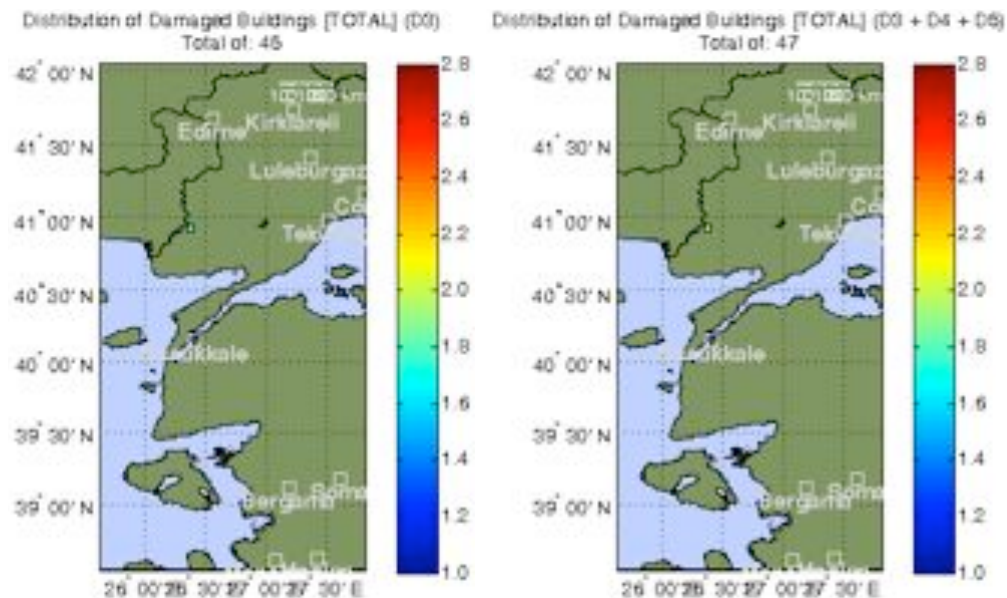


Figure 3-10. Number of Buildings with D3 (Substantial to Heavy Damage) and D3+D4+D5 (Substantial to Heavy Damage+Very Heavy Damage+Destruction) Levels on the left and right sides, respectively.

The intensity based empirical vulnerability relationship has been used for the building damage estimation in the epicentral region for the Damage Levels D1 to D5 from Slight Damage to Destruction as shown from Figure 3-9 to Figure 3-10.

The casualty estimation has been done by ELER and no casualty has been estimated as shown in the Figure 3-11.

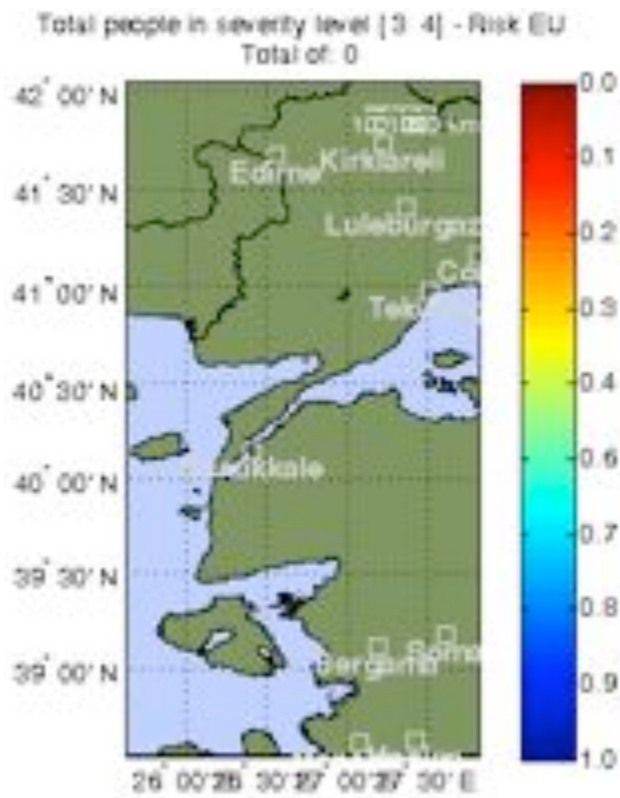


Figure 3-11. No casualty has been estimated in the region.

The spectral acceleration-displacement-based building damage estimation has been done for Istanbul. The Capacity Spectrum method has been applied. The building inventory of Istanbul has been used for the analysis and even no slight damage as shown in Figure 3-12 has been estimated for this event.

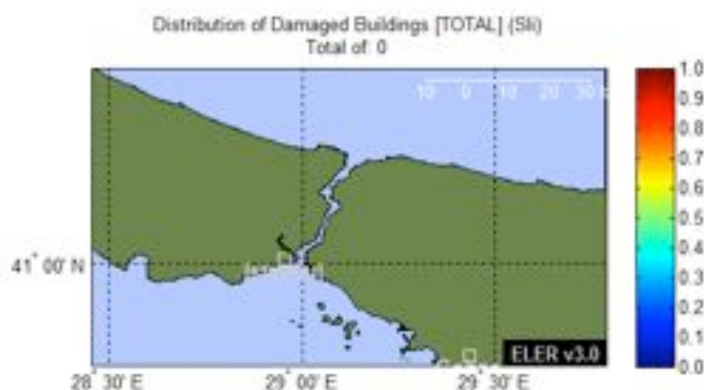


Figure 3-12. No building damage has been estimated in Istanbul due to the event.

This report has been prepared by KOERI with contributions from Mustafa Erdik, Ali Pınar, Sinan Akkar, Can Zülfiyar, Doğan Kalafat, Kivanç Kekovalı, Nurcan Meral Özel and Öcal Necmioğlu.

4. Strong Ground Motion Analysis of May 24, 2014, 09:25 (GMT) North Aegean Earthquake

Rapid Response and Early Warning networks operated by KOERI recorded a total of 75 accelerograms from the 24 May 2014 Aegean Sea, earthquake. The accelerograms were uniformly processed by applying band-pass acausal filtering. The low-pass and high-pass filter cut-offs were determined individually for each component. Figures 4-1 to 4-4 show the distributions of horizontal peak ground acceleration (PGA), peak ground velocity (PGV) as well as 5%-damped pseudo spectral accelerations (PSA) at $T = 0.2s$ and $T = 1.0s$. The distributions display the geometric means of considered ground-motion intensity measures. The maps given in these figures indicate that the mainshock PGA and PGV variations over the Istanbul area are between $1.5 \text{ cm/s}^2 < \text{PGA} < 20 \text{ cm/s}^2$ (Figure 4-1) and $0.6 \text{ cm/s} < \text{PGV} < 4 \text{ cm/s}$ (Figure 4-2), respectively. The distributions of PSA at $T = 0.2s$ and $T = 1.0s$ take values between $3 \text{ cm/s}^2 - 40 \text{ cm/s}^2$ (Figure 4-3) and $2 \text{ cm/s}^2 - 42.5 \text{ cm/s}^2$ (Figure 4-4), respectively. The observed mainshock peak ground motion and spectral amplitudes mapped for the Istanbul city are low as the source-to-site distances between the mainshock and sites are large. For this reason, the likelihood of structural damage in Istanbul due to the 24 May 2014 Aegean Sea, earthquake is negligible. The ground-motion amplitudes shown in Figures 4-1 to 5-4 tend to decrease towards stiffer sites. The amplitude distributions of PGV (Figure 4-2) and PSA at $T = 1.0s$ (Figure 4-4) mark this observation better. The observed large-amplitude pockets on the maps may bring forward the effects of local site and topography on the recorded ground motions. The maximum horizontal component PGA distribution recorded from the entire earthquake affected area that is given in Figure 4-5 indicates a measured PGA value of 65.7 mg at Mecidiye-Edirne. The distribution of maximum horizontal component PGA for the Istanbul area is given in Figure 4-6.



Figure 4-1. PGA (cm/s^2) distribution map of the Istanbul area obtained from Istanbul Early Warning and Rapid Response Networks

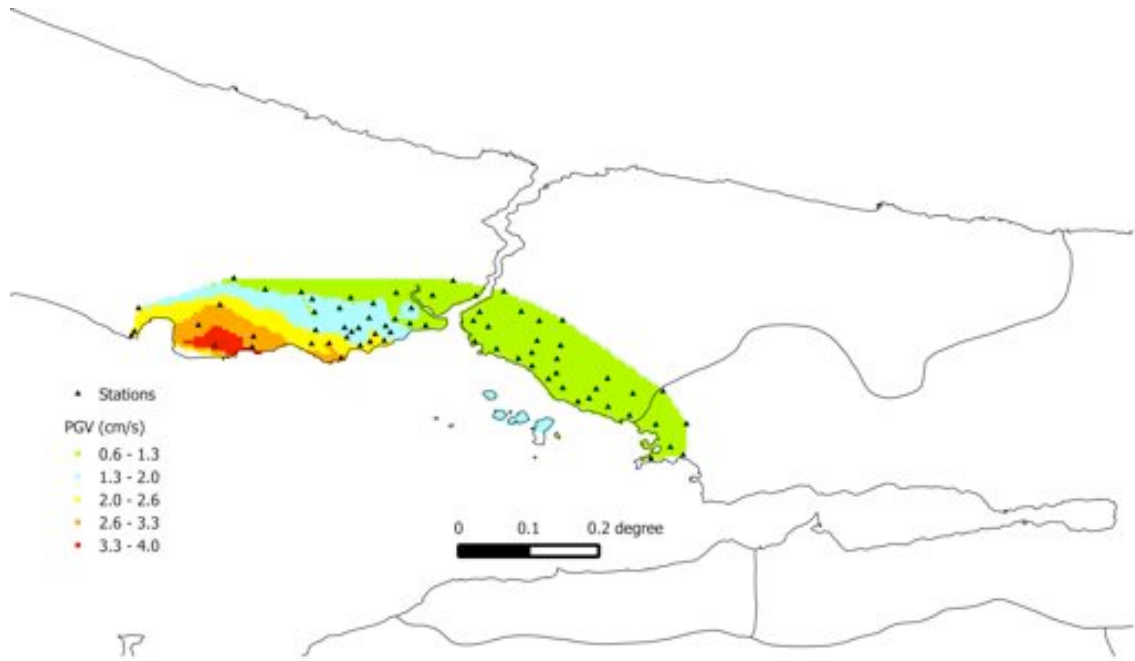


Figure 4-2. PGV (cm/s) distribution map of the Istanbul area obtained from Istanbul Early Warning and Rapid Response Networks

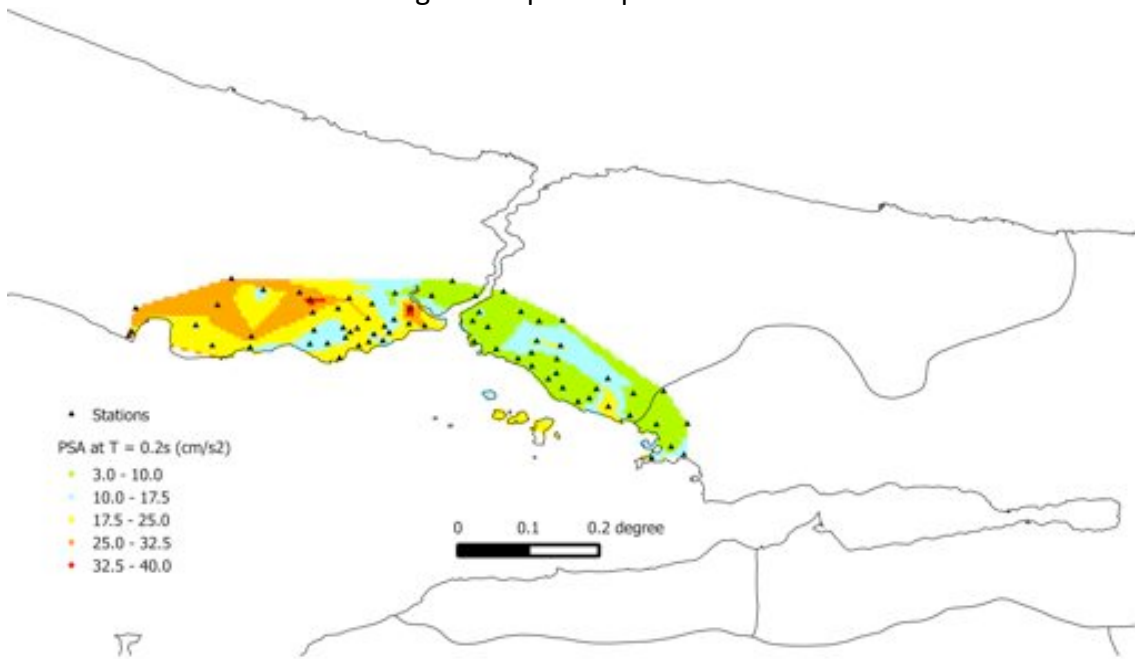


Figure 4-3. PSA (cm/s^2) at $T=0.2\text{s}$ distribution map of the Istanbul area obtained from Istanbul Early Warning and Rapid Response Networks

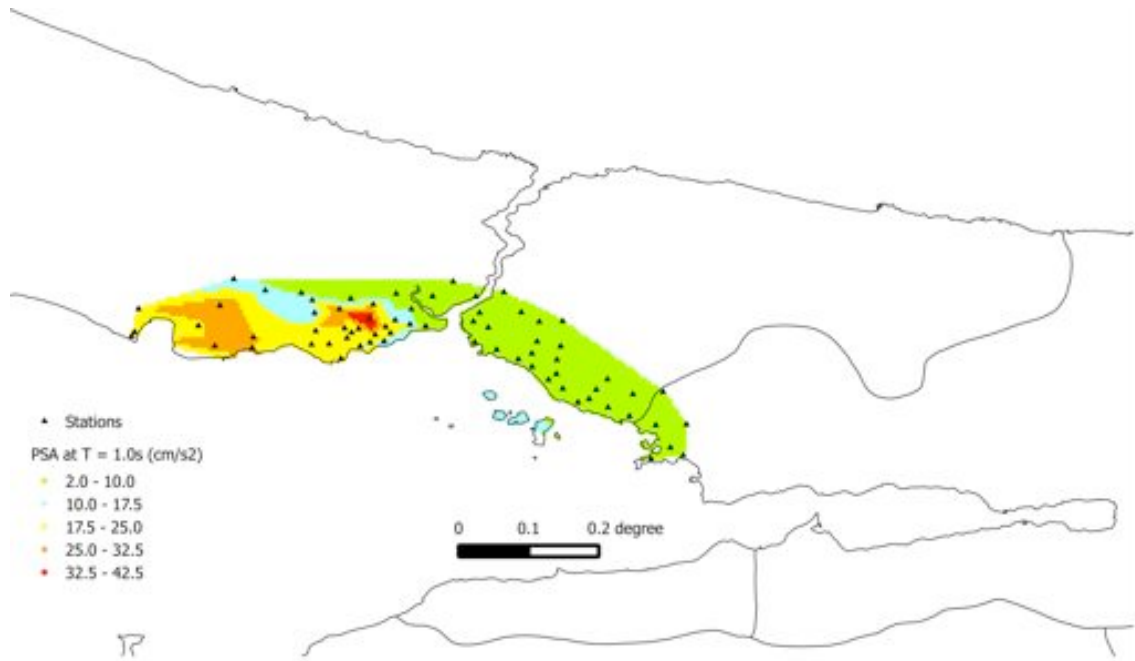


Figure 4-4. PSA (cm/s²) at T=1s distribution map of the Istanbul area obtained from Istanbul Early Warning and Rapid Response Networks

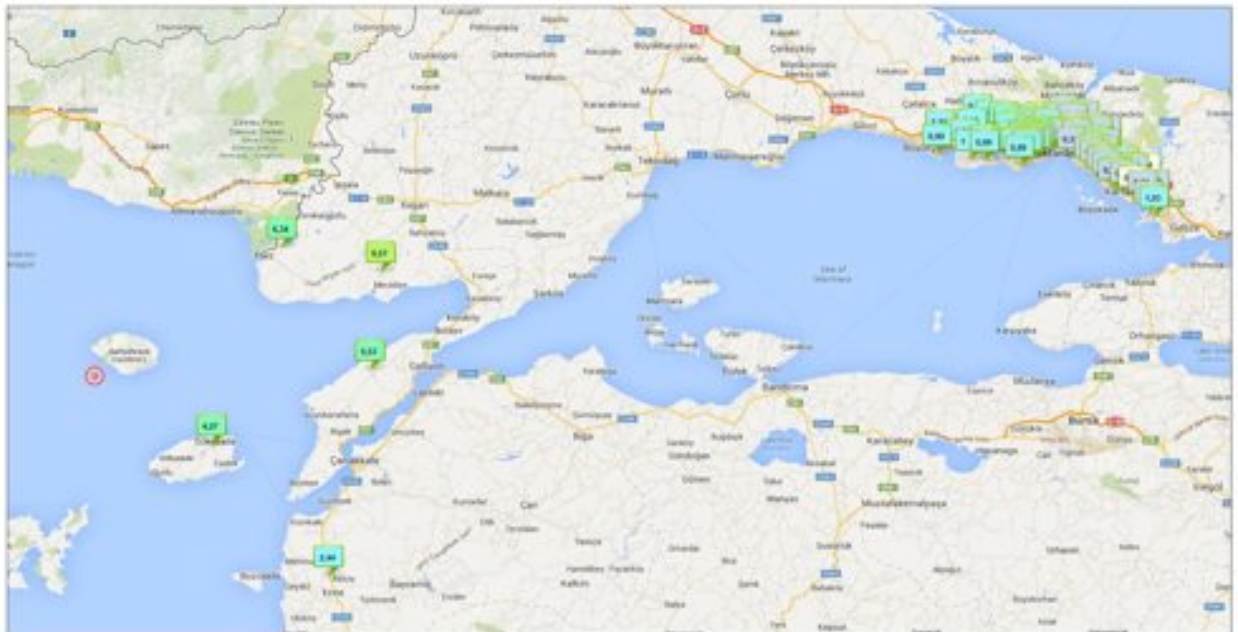


Figure 4-5. Maximum PGA (%) distribution map of the earthquake area

This report has been prepared by KOERI with contributions from Mustafa Erdik, Ali Pinar, Sinan Akkar, Can Zülfiyar, Doğan Kalafat, Kıvanç Kekovalı, Nurcan Meral Özel and Öcal Necmioğlu.

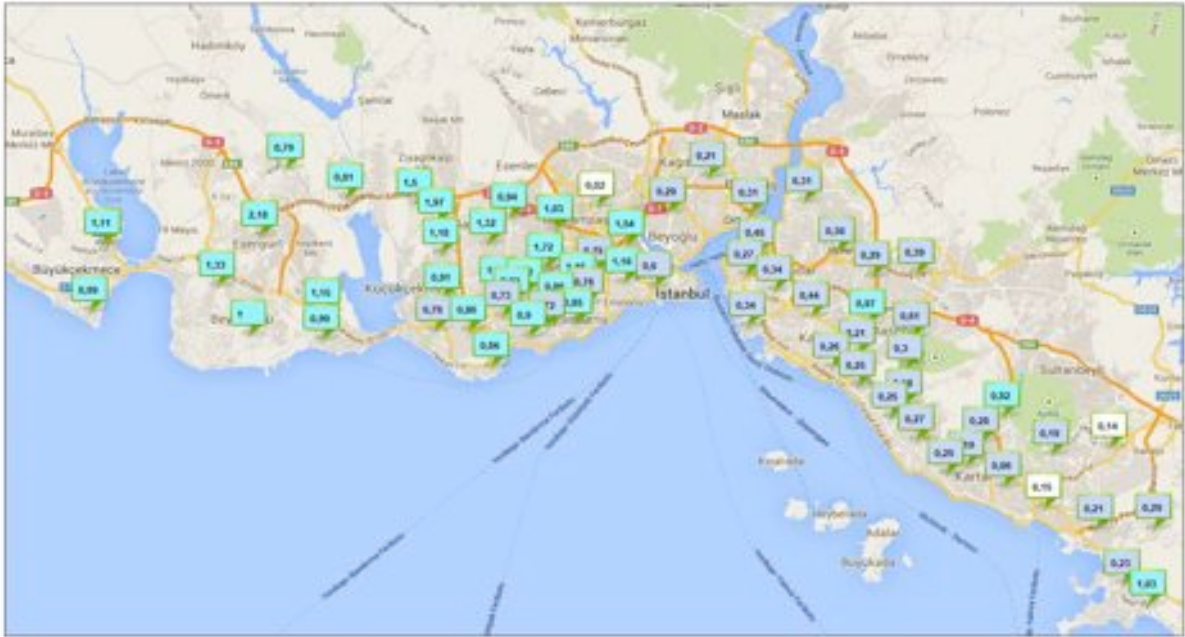


Figure 4-6. Maximum PGA (%) distribution map of the Istanbul area

5. Source Features of the May 24, 2014, 09:25 (GMT) North Aegean Earthquake

Aftershock distribution

The most prominent feature of the earthquake is the widespread distribution of the aftershocks. The routine fast locations carried out by the National Earthquake Monitoring Center (NEMC) of KOERI portrays a lateral variation of longitudes between 25.0°E and 26.2°E . This corresponds to approximately 120 km fault rupture length if all the aftershocks take place along the

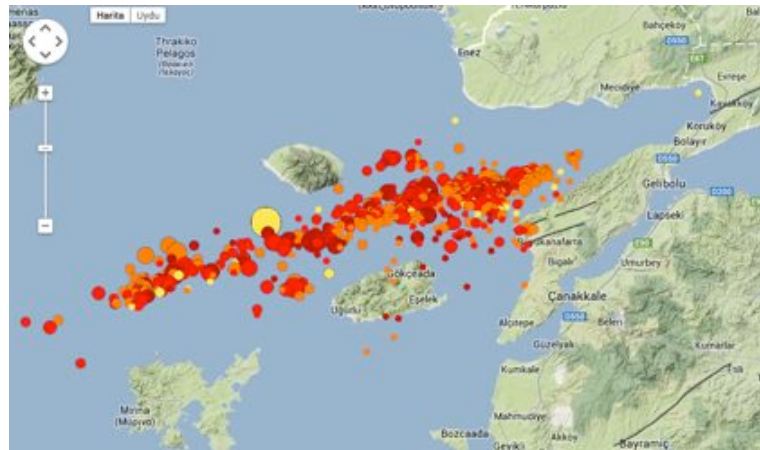


Figure 5-1. The aftershock distribution of events between May 24th and May 30th, 2014.

ruptured fault plane. Using the USGS estimated seismic moment magnitude of $M_w=6.9$ and the relation between fault rupture length and moment magnitude of Wells and Coppersmith (1994), $(\text{Log}(L)=(M_w-5.16 \pm 0.13)/1.12 \pm 0.08)$ yields a rupture length between 35-60 km. Thus estimated rupture length is a few times shorter than the rupture derived from the aftershock distribution (Figure 5-1).

This report has been prepared by KOERI with contributions from Mustafa Erdik, Ali Pinar, Sinan Akkar, Can Zülfiyar, Doğan Kalafat, Kivanç Kekovalı, Nurcan Meral Özel and Öcal Necmioğlu.

Teleseismic Bodywave modeling

Using the complex teleseismic bodywave records generated by the earthquake and the method developed by Kikuchi and Kanamori (2003) we estimated the seismic moment release on each subfault grid distributed along the strike and dip of the ruptured fault plane (Figure 5-2). The grid size of 10x5 km was chosen as 10 km along the strike and 5 km along the dip of the fault plane. The inversion results yield a seismic moment of $M_0=2.9 \times 10^{19}$ Nm ($M_w=6.9$) and approximately 30 sec source rupture duration. The size and arrow of the vectors (rake) shown on the fault plane (Figure 5-2) characterize the seismic moment tensor derived for each grid point. The rakes illustrated in Figure 5-2 suggests that the region to the west of the epicenter experienced mainly strike-slip motion while to the east considerable dip-slip component contributed to the motion on the fault plane.

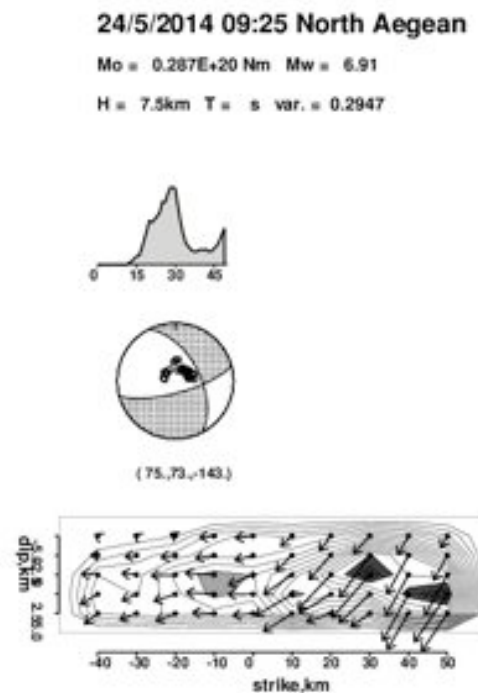


Figure 5-2. 2D slip distribution along the ruptured fault plane.

Coulomb Failure Stress Changes

The slip distribution model portrayed in Figure 5-2 was used to estimate the co-seismic static stress changes associated with the mainshock. In our calculations we used a frictional coefficient of 0.3 which is one of the parameters affecting the spatial distribution of the Coulomb stress changes for the optimally oriented fault planes. Considering the predominantly strike slip mechanism for most of the events in North Aegean we used a regional stress tensor appropriate for strike-slip tectonic regimes. The azimuth of the maximum principle axis was fixed at 290 degree. The results with the fixed parameters are shown in Figure 5-3. Here, the red colour indicates the areas of increased stress changes and the blue regions show the region where the stress changes are negative.

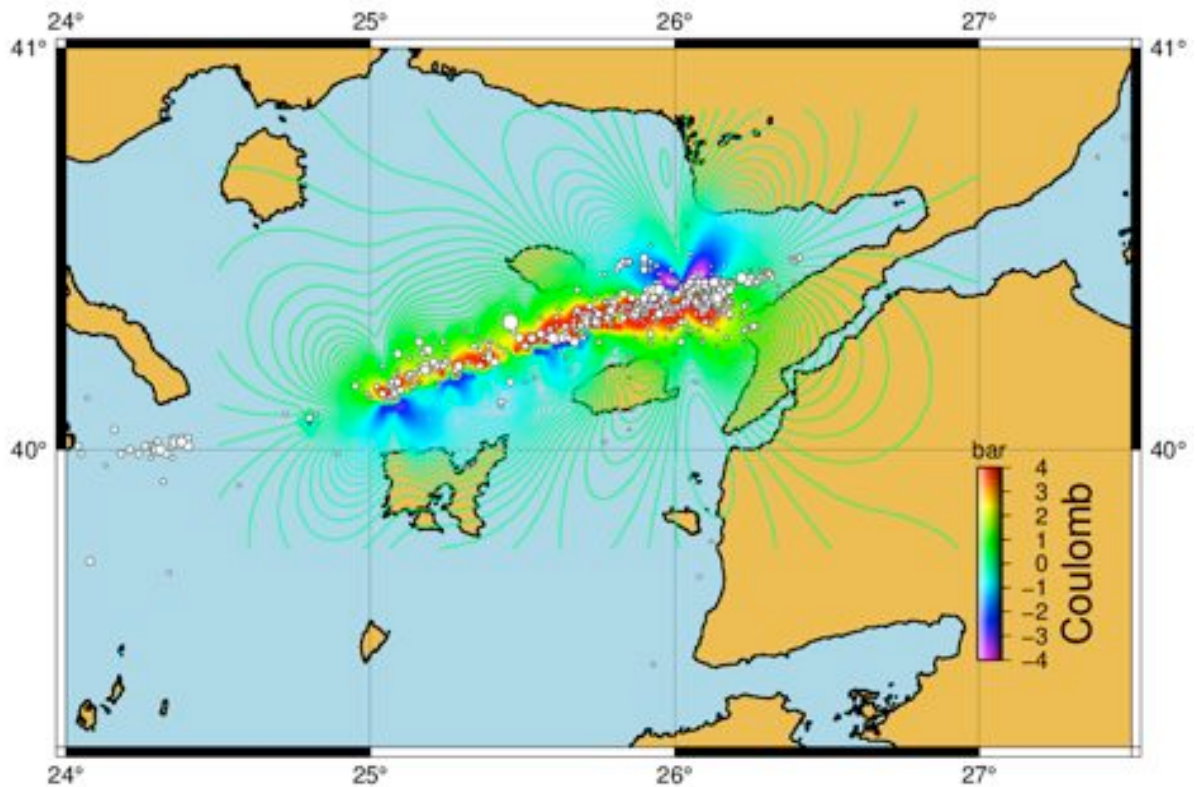


Figure 5-3. Coulomb stress changes associated with the mainshock. The aftershocks tend to take place at regions of increased stress. Note the southward extension of the aftershock area and the area of increased stress to the east of the epicenter where dip-slip component was derived.

Meanwhile, the North Aegean earthquake triggered a discussion among the Turkish earth scientists on whether the increased static stress changes will trigger the expected large Marmara earthquake.

We constructed an east-west cross-section of the Coulomb stress changes based on the results presented in Figure 5-3 so as to explore the eastward extension of the stress changes toward the Saros bay (Figure 5-4). Such a cross section reveals that the Coulomb stresses exponentially decrease starting from the eastern termination of the rupture toward the east. Besides, it is obvious from Figure 5-4 that the aftershocks taking place to the east of the mainshock area are the events triggered by the static stress increase rather than events taking place on a ruptured plane. Most of the aftershocks concentrate at the region where the stress increase is between 0.5-3.0 bars. The region where the stress is less than 0.5 bar the aftershock activity diminishes.

The fault segments to the east of the ruptured area were broken by the 1912 Şarköy-Mürefte ($M_w=7.4$) and the 1975 Saros bay ($M_w=6.3$) earthquakes. The surface ruptures on the Ganos fault segment, extending from Saros bay towards the Marmara sea, associated with the 1912 earthquakes reveal that the coseismic maximum displacements were in the range between 4 to 5 m (Aksoy et al., 2010). This in turn implies that the Ganos fault segment is a strong fault, i.e., strong enough to bear stresses capable to generate 5 m slip.

On the other hand, the GPS study carried out by Ergintav et al. (2007) shows that the slip rate along the Ganos fault segment is about 17 mm/yr. Thus, the level of strain already accumulated on that fault is far below the maximum bearable stress range of the Ganos segment. Thus, considering all these facts and the stress increases on the Ganos fault caused by the last North Aegean earthquake one may claim that the increased seismic risk is within the range already predicted by the seismic hazard maps.

By virtue of the fact that, the fault segments expected to be ruptured by the impending Marmara earthquake occur further east of the Ganos fault, the coseismic static stress loading caused by the last North Aegean earthquake on those fault segments should be negligible in the order of milibars (Figure 5-3 and Figure 5-4).

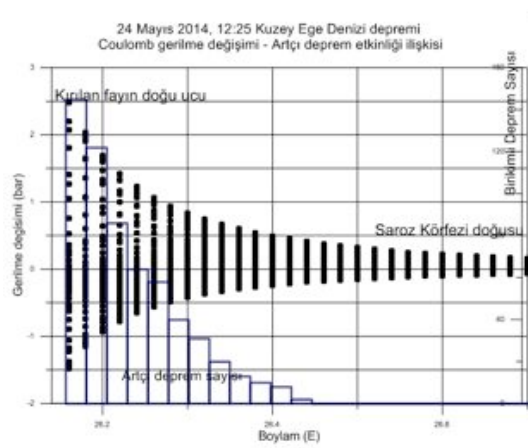


Figure 5-4. A relation between the number of aftershocks and the stress changes to the east of the ruptured plane (the black dots are the stresses and the histogram show the number of the aftershocks).

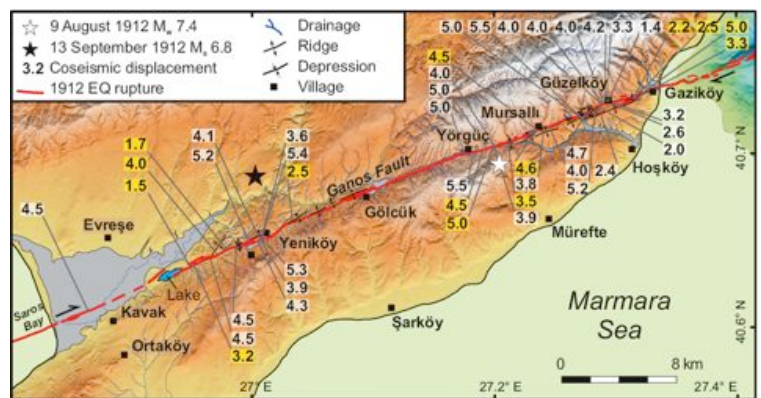


Figure 5-5. Lateral displacements measured from the surface ruptures associated with the 1912 Şarköy-Mürefte earthquake (Aksoy et al., 2010).

6. Earthquake Information System

244 users of the Android application “Earthquake Information System” have reported their observations to KOERI within 30 minutes of earthquake origin time. A preliminary analysis has been made on how this earthquake was felt in the region based on this information. Red color in the figure indicates stronger felt ground shaking. In particular, this map is very well in accordance with the automatically produced Shake-Map of KOERI. The earthquake has been felt with VI intensity in Gökçeada (Imbros), V intensity (Imbros), and IV intensity in Thrace and Northwest Anatolia where the density of the users increases in the latter. The mean intensity is V+. We thank all users for the feedback provided.

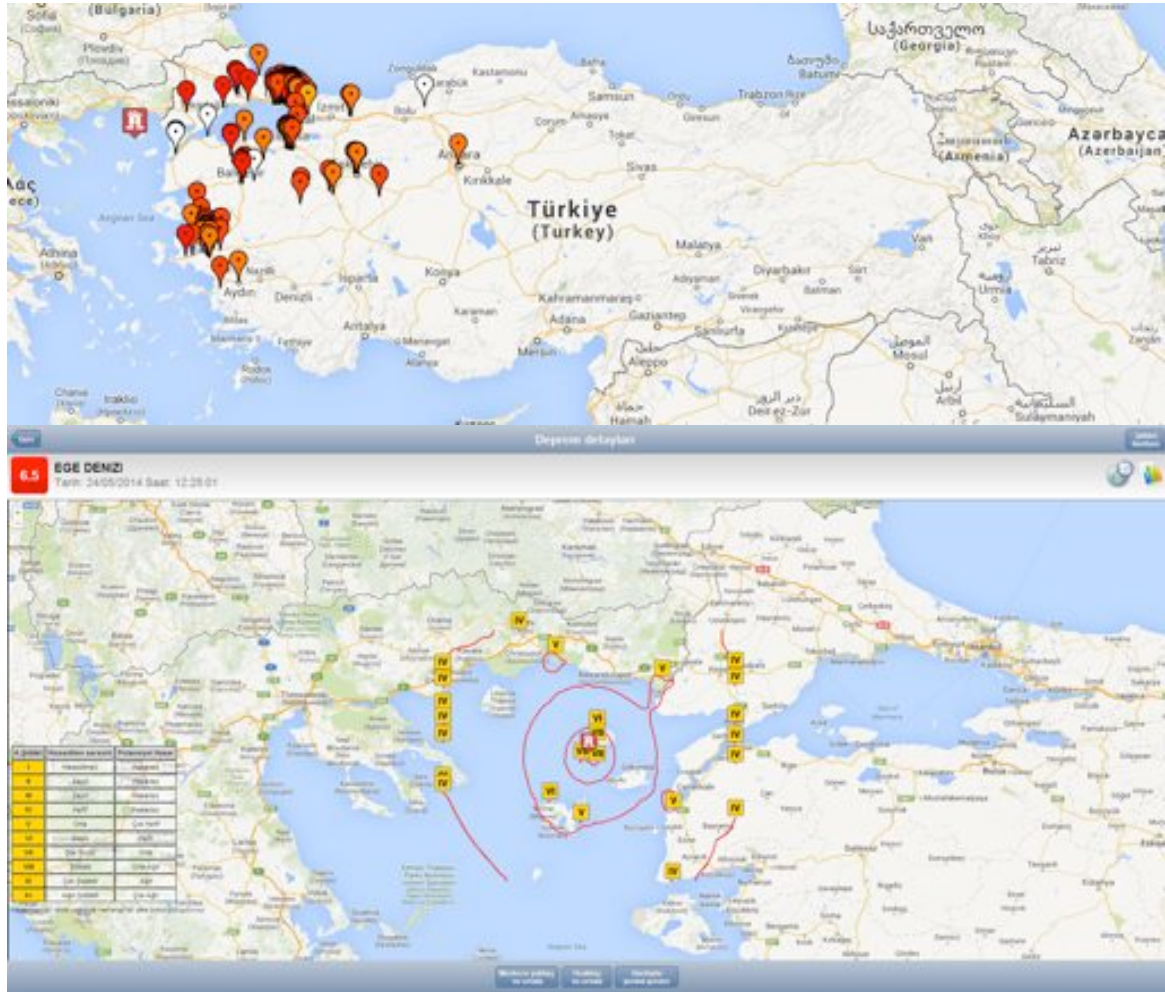


Figure 6-1. Intensity Map produced based on the feedback given by the KOERI Android Application “Earthquake Information System”

7. Tsunami Messages

KOERI is a Candidate Tsunami Watch Provider of Tsunami Warning System in the North-eastern Atlantic, the Mediterranean and connected seas region UNESCO-IOC-ICG/NEAMTWS) providing services to its subscribers in the Eastern Mediterranean, Aegean and Black Seas since 1 July 2012. A Tsunami WATCH and ADVISORY Message has been disseminated based on the ICG/NEAMTWS Decision Matrix 18 minutes after origin time. This initial message was followed by a CANCELLATION Message disseminated 3 h 14 min after origin time based on the sea-level measurements at Bodrum tide-gauge station in Turkey. The sea-level recording of 16 cm at the Gökçeada (Imbros) tide-gauge station 5 min after earthquake origin time, which was not available in real-time at the time of the event due to a satellite communication system, could be associated to a tsunami generated by this earthquake.

Decision matrix for the Mediterranean						
Depth (km)	Epicentre location	Earthquake magnitude (M_w)	Tsunami potential	Type of tsunami message		
				Local	Regional	Basin-wide
< 100	Offshore or close to the coast (≤ 40 km inland)	5.5 – 6.0	Weak potential for a local destructive tsunami	Advisory	Information	Information
		6.0 – 6.5	Potential for a destructive local tsunami	Watch	Advisory	Information
	Offshore or close to the coast (≤ 100 km inland)	6.5 – 7.0	Potential for a destructive regional tsunami	Watch	Watch	Advisory
		≥ 7.0	Potential for a destructive basin-wide tsunami	Watch	Watch	Watch
≥ 100	Offshore or inland (≤ 100 km)	≥ 5.5	No tsunami potential	Information	Information	Information

No message if the earthquake is localised inland beyond 100 km distance; no message if $M_w < 6.5$ and distance to the coast > 40 km; no message if $M_w < 5.5$.

Figure 7-1. ICG/NEAMTWS Tsunami Potential DecisionMatrix for the Mediterranean

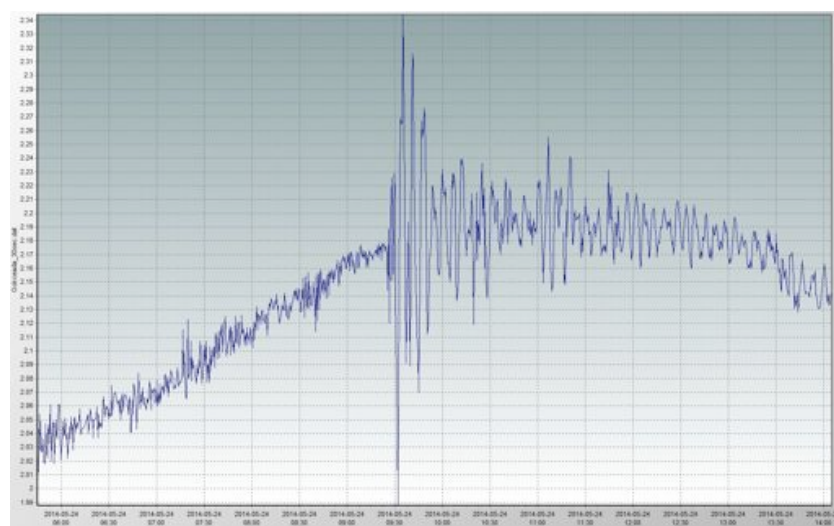


Figure 7-2. Sea-level record indicating a 16 cm tsunami at Gökçeada (Imbros) tide-gauge station in Turkey (measured relative to the normal sea level as indicated in the ICG/NEAMTWS Interim Operational User's Guide).